Magnetic and magnetoelastic properties of $LiDyF_4$ single crystals

2013 J. Phys.: Conf. Ser. 478 012026

(http://iopscience.iop.org/1742-6596/478/1/012026)

Journal of Physics: Conference Series **478** (2013) 012026 doi:10.1088/1742-6596/478/1/012026

Magnetic and magnetoelastic properties of $LiDyF_4$ single crystals

I V Romanova[1,2], S L Korableva[1], V I Krotov[3], B Z Malkin[1], I R Mukhamedshin[1,2], H Suzuki[2], M S Tagirov[1]

[1]Kazan Federal University, Kazan, 420008, Kremlevskaya 18, Russia
[2]Kanazawa University, Kanazawa, 920-11, Kakuma-machi, Japan
[3]Kazan State Power Engineering University, Kazan, 420066, Krasnoselskaya, 51, Russia

E-mail: Irina.Choustova@kpfu.ru

Abstract. Temperature and magnetic field dependences of the magnetization of $LiDyF_4$ single crystal were measured with a dc-SQUID magnetometer. The longitudinal magnetostriction was measured by the capacitance-bridge method. A giant compression of the crystal lattice up to 0.1% was observed in the magnetic field of 1 T along the [110] direction at 4.2 K. Experimental data are well reproduced by simulations based on the microscopic models of the single-ion magnetoelastic and inter-ion multipole interactions.

1. Introduction

Double lithium-rare earth fluorides which crystallize in the tetragonal scheelite structure attract a lot of interest as model objects in physics of dipolar magnets [1]. The unit cell of $LiLnF_4$ contains two magnetically equivalent trivalent lanthanide ions at sites with the S_4 point symmetry. Single crystal $LiDyF_4$ is a dipolar XY-antiferromagnet with Dy^{3+} magnetic moments normal to the crystal symmetry axis (T_N=0.62 K) [1]. It was shown recently that $LiDyF_4$ is a promising material for Faraday rotators in the ultraviolet-visible wavelength region [2]. The analysis of magnetic dipolar and exchange interactions between the Dy^{3+} ions and of the magnetic structure was presented in [3] based on the measurements of the low temperature specific heat. The energy levels crossover effects in strong pulse magnetic fields on the magnetization of $LiDyF_4$ were studied in [4].

The main goal of the present study was to elucidate the role of magnetoelastic and multipole interactions in formation of the magnetization, magnetostriction and the energy level structure of Dy^{3+} ions in $LiDyF_4$ crystals in the external magnetic fields.

2. Experimental details

Single crystals of $LiDyF_4$ were grown by Bridgeman-Stockbarger method. The samples were oriented by means of X-ray diffractometer. The sample used for magnetization measurements was shaped by polishing as a sphere to acquire a definite demagnetizing factor. It was fixed in Stycast 1266 epoxy (the accuracy of orientation was ±3°) in order to prevent rotation in strong magnetic fields. Temperature and field dependences of the single crystal magnetization in the temperature range of 2 - 300 K and the magnetic fields in the range of 0 - 5 T applied along and perpendicular to the c-axis were measured using a dc-SQUID magnetometer MPSM-2 (Quantum Design).

The measured temperature and field dependences of the magnetization in $LiDyF_4$ single-crystals are compared with the results of simulations in figures 1 and 2.

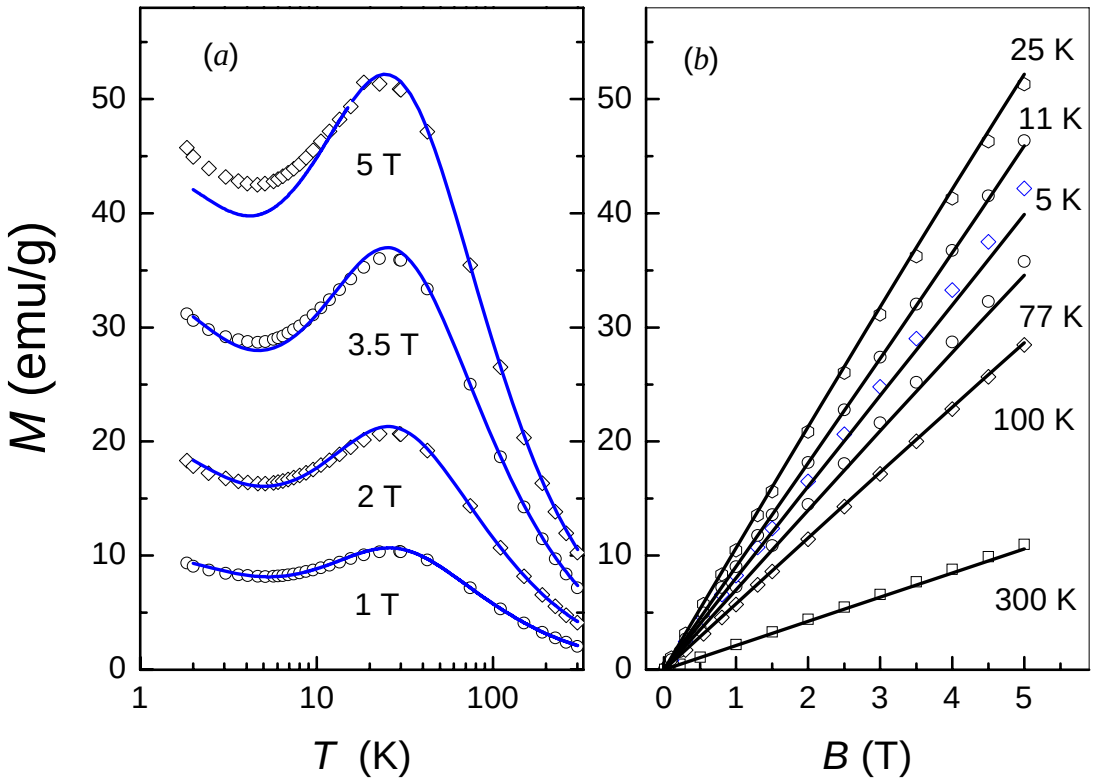

Figure 1. Measured (symbols) and calculated (solid curves) temperature (*a*) and magnetic field (*b*) dependences of the magnetization in $LiDyF_4$ for different values of magnetic fields parallel to the crystal c-axis and temperatures.

The longitudinal magnetostriction was measured at the temperature 4.2 K as a function of the external magnetic field varied from zero up to 1 T. The measurements were performed by the capacitance-bridge method [5]. The crystal was placed in a helium cryostat at the center of a superconducting solenoid and was connected to the measuring device by means of a quartz rod. The signals induced by the change of the sample length with increase of the magnetic field were directly registered with an X-Y recorder; a voltage proportional to the current through the solenoid was applied to the X input. The sign of the deformation was determined and the sensitivity of the apparatus was calibrated by means of control measurements of the magnetostriction of the polycrystalline nickel. To obtain the measurement results independent on the displacement of the sample under the action of the torque due to the interaction of the anisotropic magnetic moment of the Dy^{3+} ions with the magnetic field, the sample was secured with vacuum grease or silicone oil. The experiments were performed on cylindrical samples of 5-6 mm diameter and 6-10 mm length, with finely polished flat and parallel surfaces. The axes of the samples were oriented along the crystallographic directions [100] or [110] by the X-ray diffraction with an accuracy not worse than 3°. The results of the measurements are presented in figure 3.

3. Experimental results and discussion: magnetization and magnetostriction in $LiDyF_4$

The measured temperature and magnetic field dependences were analyzed by making use of the effective single-ion Hamiltonian

$$H_{eff} = H^{(0)} + H^{(P)} \tag{1}$$

where

$$H^{(0)} = H_0 + H_{cf} + H_Z, \tag{2}$$

$$H^{(P)} = \{\sum_{\alpha\beta} B_{eff,\alpha\beta} e_{\alpha\beta} - < O >_0 : [\frac{n}{v} \sum_{rr'} D_{eff,\alpha}(r) \hat{a}^{-1}_{\alpha\beta}(r,r') D_{eff,\beta}(r') + \lambda : (1 + q : \lambda)^{-1}]\} : O \tag{3}$$

operating in the space of states of the $4f^9$ electronic configuration of the Dy^{3+} ion. Here H_0 is the free ion standard Hamiltonian defined by the parameters of electrostastic, spin-orbit and interconfigurational interactions presented in [6]. The crystal field Hamiltonian in the crystallographic system of coordinates is determined by the set of seven crystal field parameters B^k_p,

$$H_{cf} = B^0_2 O^0_2 + B^0_4 O^0_4 + B^4_4 O^4_4 + B^{-4}_4 O^{-4}_4 + B^0_6 O^0_6 + B^4_6 O^4_6 + B^{-4}_6 O^{-4}_6, \tag{4}$$

where O^k_p are linear combinations of spherical tensor operators [7]. The third term in (2) is the electronic Zeeman energy in the external magnetic field $\boldsymbol{B}$, $H_Z = \mu_B \mathbf{B}(\mathbf{L} + 2\mathbf{S})$, here μ_B is the Bohr magneton, $\boldsymbol{L}$ and $\boldsymbol{S}$ are orbital and spin moments of an ion, respectively.

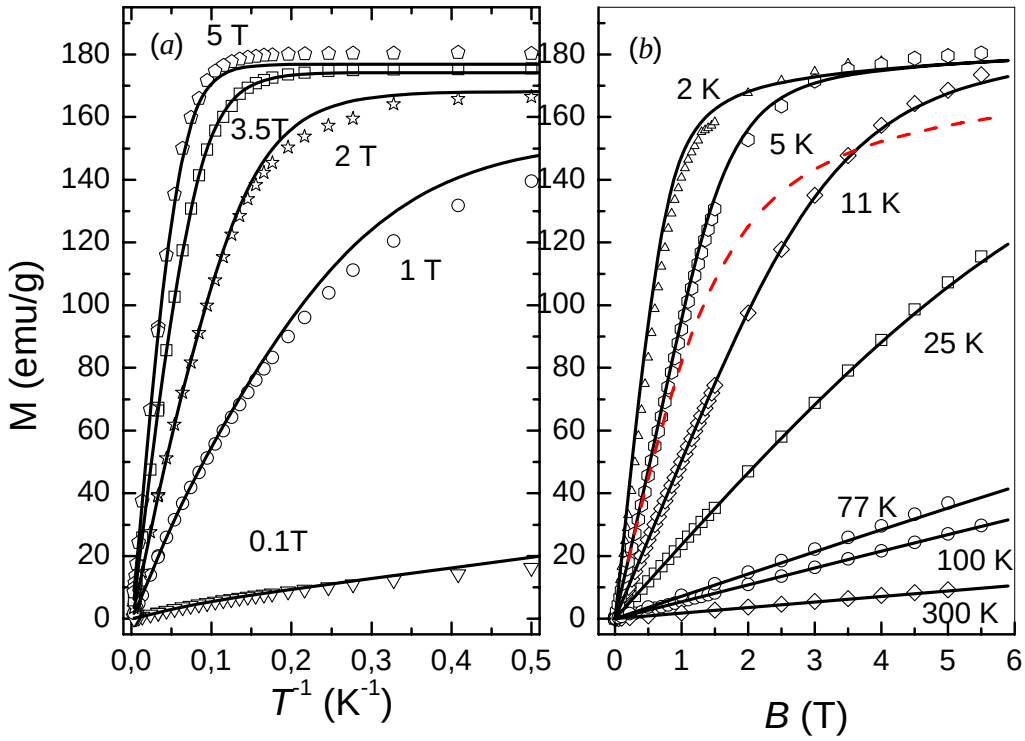

Figure 2. Measured (symbols) and calculated (solid curves) temperature (*a*) and magnetic field (*b*) dependences of the magnetization in $LiDyF_4$ for the magnetic fields parallel to the crystal *a*-axis. The dashed curve represents the calculated magnetization at *T*=5 K when the electron-deformation interaction is not taken into account.

The Hamiltonian (3) contains terms corresponding to multipole interactions between the Dy^{3+} ions and the electron-deformation interaction. Here a colon symbol means a convolution over the indices of the spherical tensors ($\sum_{pk} A_p^k O_p^k = A:O$), n=2 is the number of the magnetically equivalent paramagnetic ions in the unit cell with a volume v. The matrix q is the generalized multipole susceptibility depending on temperature T:

$$q_{pp'}^{kk'} = \frac{1}{k_B T}[< O_p^k >_0 < O_{p'}^{k'} >_0 - \sum_i \langle \psi_i | \rho O_p^k | \psi_i \rangle \langle \psi_i | O_{p'}^{k'} | \psi_i \rangle] + \sum_{i,j \neq i} (\varepsilon_i - \varepsilon_j)^{-1} [\langle \psi_i | \rho O_p^k | \psi_j \rangle \langle \psi_j | O_{p'}^{k'} | \psi_i \rangle + \langle \psi_i | \rho O_{p'}^{k'} | \psi_j \rangle \langle \psi_j | O_p^k | \psi_i \rangle], \quad (5)$$

here ε_i and ψ_i are eigenvalues and eigenfunctions of the Hamiltonian $H^{(0)}$, k_B is the Boltzmann constant, a symbol <...>$_0$ means quantum statistical averaging with the equilibrium density matrix $\rho = \exp(-H^{(0)} / k_B T) / Tr(\exp(-H^{(0)} / k_B T))$. The electron-deformation interaction linear in components of the deformation tensor $e_{\alpha\beta}$ and the sublattice displacements $w_\alpha(r)$ ($r = 1 \div 11$) is defined by the parameters $B_{p,\alpha\beta}^k$ and $D_{p,\alpha}^k(r)$:

$$H_{el-def} = \sum_{pk} [\sum_{\alpha\beta} B_{p,\alpha\beta}^k e_{\alpha\beta} + \sum_{\alpha,r} D_{p,\alpha}^k(r) w_\alpha(r)] O_p^k . \quad (6)$$

These parameters are renormalized due to coupling between the macro- and microdeformations determined by the tensors $b_{\alpha\beta,\gamma}(r)$ [8, 9] and by the multipole interactions. In particular, we use in (3) the effective parameters of the electron-deformation interaction

$$D_{eff\ p,\alpha}^k(r) = \sum_{p'k'} [(1 + \lambda : q)^{-1}]_{pp'}^{kk'} D_{p',\alpha}^{k'}(r) , \quad (7)$$

$$B_{eff\ p,\alpha\beta}^{\ k} = \sum_{p'k'} [(1 + \lambda : q)^{-1}]_{pp'}^{kk'} \hat{B}_{p',\alpha\beta}^{k'} , \quad (8)$$

where

$$\hat{B}_{p,\alpha\beta}^k = B_{p,\alpha\beta}^k - \sum_{rr'\gamma\delta} b_{\alpha\beta,\gamma}(r) a_{\gamma\delta}^{-1}(r,r') D_{p,\delta}^k(r') , \quad (9)$$

and $a_{\alpha\beta}(r,r')$ is the dynamic matrix of the crystal lattice at the Brillouin zone centre.

The multipole interactions were considered in the framework of the self-consistent field approximation neglecting second-order terms in fluctuations $O_p^k(Ls) - < O_p^k(Ls) >$ of the operators $O_p^k(Ls)$ relating to ions at sites s in unit cells L. The corresponding average values $< O_p^k(Ls) >=< O_p^k >$ were eliminated from the explicit expression for the free energy F of the crystal by making use of the equilibrium conditions $\partial F / \partial < O_p^k >= 0$. We assume that the multipole interactions are induced by the phonon exchange between the paramagnetic ions. In this case components of the matrix λ introduced in (3) can be written as follows [10]:

$$\lambda_{pp'}^{kk'} = \frac{1}{n} \sum_{ss'} \left[\sum_{j_o} \frac{B_p^k(s,0 j_o) B_{p'}^{k'}(s',0 j_o)}{\omega_{\mathbf{0} j_o}^2} - \frac{\delta_{ss'}}{N} \sum_{\mathbf{q}j} \frac{B_p^k(s,\mathbf{q}j) B_{p'}^{k'}(s',-\mathbf{q}j)}{\omega_{\mathbf{q}j}^2} \right], \quad (10)$$

here the sum in the first term is taken over optical branches of the lattice vibrational spectrum, N is the number of the cells, $\omega_{\mathbf{q}j}$ is the frequency of a phonon with the wave vector $\boldsymbol{q}$, $B_p^k(s,\mathbf{q}j)$ are parameters of the electron-phonon interaction linear in lattice normal coordinates.

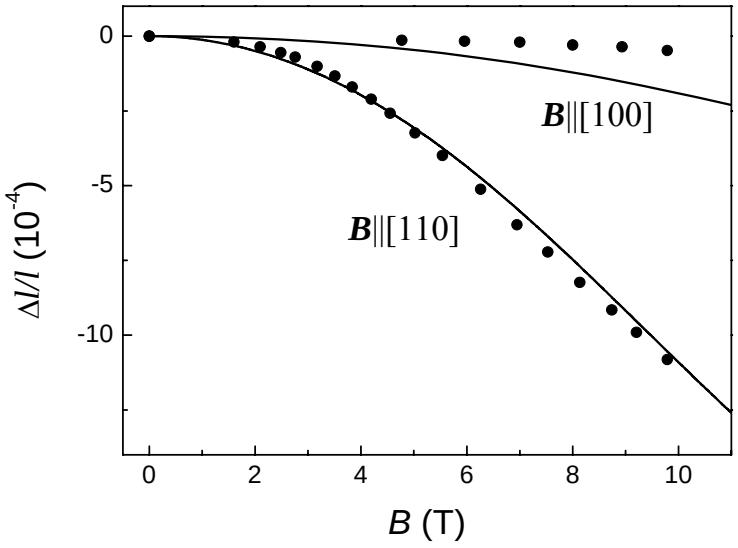

Figure 3. Measured (symbols) and calculated (solid curves) longitudinal magnetostriction of $LiDyF_4$ in the external magnetic fields along the [100] and [110] directions, T=4.2 K.

The free energy of the elastically deformed single crystal (per unit cell) written in second order in the perturbation (3) has the following form:

$$F = \frac{v}{2}\mathbf{eCe} + nF_0 - \frac{n}{2} < O >_0 : [\lambda : (1+q:\lambda)^{-1} + \frac{n}{v}\sum_{rr'}\hat{\mathbf{D}}(r)\hat{\mathbf{a}}^{-1}(r,r')\hat{\mathbf{D}}(r')] : < O >_0 + n < O >_0 : \mathbf{B}_{eff}\mathbf{e} \quad (11)$$

where F_0 is the free energy of a single ion with the Hamiltonian $H^{(0)}$ and

$$C_{\alpha\beta\gamma\delta}(T,\mathbf{B}) = C^{(0)}_{\alpha\beta\gamma\delta} + \frac{n}{v}\hat{B}_{\alpha\beta} : q : (1+\lambda:q)^{-1} : \hat{B}_{\gamma\delta} \quad (12)$$

are renormalized elastic constants.

The calculations of the average magnetic moments

$$\mathbf{M} = \mu_B Tr[(\mathbf{L}+2\mathbf{S})\exp(-H_{eff}/k_BT)] / Tr[\exp(-H_{eff}/k_BT)] \quad (13)$$

in the present work were carried out by making use of the numerical diagonalization of the Hamiltonian (1) in the total space of 2002 electronic states of the $4f^9$ configuration. The magnetic dipolar interactions between the Dy^{3+} ions were accounted for by introducing the local magnetic fields

$$\mathbf{B}_{loc}(s) = \mathbf{B} + \sum_{s'}[\mathbf{Q}(s,s') - \frac{4\pi}{3v}N_d]\mathbf{M}(s'), \quad (14)$$

where $\mathbf{M}(s)$ is the magnetic moment of an ion belonging to the s-sublattice, N_d is the demagnetizing factor and $\mathbf{Q}(s,s')$ are the corresponding lattice sums.

To analyze the magnetostriction, we calculated the relative changes of the crystal size $\Delta l / l = \sum_{\alpha\beta} n_\alpha n_\beta e_{\alpha\beta}$ along a unit vector with directional cosines n_α where variations of components of the deformation tensor with the magnetic field were determined from the minimum condition of the free energy (11):

$$\mathbf{e}(\mathbf{B}) = -\frac{n}{\nu}[\mathbf{SB}_{eff} :< O >_0 \big|_{\mathbf{B}} - \mathbf{SB}_{eff} :< O >_0 \big|_{\mathbf{B}=0}] \quad (15)$$

(here $\mathbf{S} = \mathbf{C}^{-1}$ is the compliance tensor).

Table 1. Parameters of the interaction between the Dy^{3+} ions and lattice deformations of B_g symmetry in $LiDyF_4$ (cm^{-1}). The effective parameters are given for zero magnetic field and T=4.2 K.

	p k							
	2 2	2 -2	4 2	4 -2	6 2	6 -2	6 6	6 -6
$\hat{B}_p^k(B_g^1)$	1997	2355	-887	1200	-135	-427	-731	-691
$B_{eff\ p}^{\ k}(B_g^1)$	1617	3817	-1497	1766	-322	-549	-614	-1022
$\hat{B}_p^k(B_g^2)$	4114	-1144	-1120	1652	-528	-375	-841	-878
$B_{eff\ p}^{\ k}(B_g^2)$	4614	-4406	337	168	-126	-4	-997	-98

The calculations are essentially simplified when making use of symmetry properties of a system. Indeed, we worked with linear combinations of the deformation tensor $e(A_g^1) = e_{zz}$, $e(A_g^2) = (e_{xx} + e_{yy})/2$, $e(B_g^1) = e_{xx} - e_{yy}$, $e(B_g^2) = e_{xy}$, $e_1(E_g) = e_{xz}$, $e_2(E_g) = e_{yz}$ and the sublattice displacements corresponding to irreducible representations A_g, B_g, E_g of the lattice factor group C_{4h}. In particular, the magnetic field directed along the c-axis induces only totally symmetric A_g deformations, while A_g and rhombic B_g deformations are induced by fields perpendicular to the c-axis.

Table 2. Parameters of the mutipole interactions $\lambda_{ij} = \lambda_{ji}$ (cm^{-1}).

i \ *j*	1	2	3	4	5	6	7	8
1	-72.02	-54.76	48.49	-54.84	10.18	26.5	22.5	29.96
2		62.98	-17.76	10.88	-7.127	3.516	16.07	-6.565
3			-2.0	4.572	-3.149	-0.482	-13.64	-4.882
4				-28.56	-1.775	4.771	14.09	1.137
5					-1.935	-1.158	-4.147	-1.7
6						-1.932	-5.529	-6.8
7							-6.556	-9.053
8								-6.287

As follows from the previous studies of magnetoelastic effects in double lithium-rare earth fluorides [1, 9], interactions of rare earth ions with the lattice deformations of the B_g symmetry play the dominant role. The corresponding terms in the Hamiltonian (6) involve only eight operators $O_2^2 = O_1$, $O_2^{-2} = O_2$, $O_4^2 = O_3$, $O_4^{-2} = O_4$, $O_6^2 = O_5$, $O_6^{-2} = O_6$, $O_6^6 = O_7$, $O_6^{-6} = O_8$. The corresponding parameters of the multipole interaction, elements of the matrix λ, in accordance with (10) where we neglect dependences of the phonon frequencies in the optical branches on the wave vectors, can be written as

$$\lambda_{ij} = \sum_{\upsilon=1:5} \frac{B_i(B_g^\upsilon)B_j(B_g^\upsilon)}{\omega(B_g^\upsilon)^2} - \sum_{\upsilon=1:4} \frac{B_i(A_u^\upsilon)B_j(A_u^\upsilon)}{\omega(A_u^\upsilon)^2} - \frac{1}{N}\sum_{\mathbf{q}j_a} \frac{B_i(1,\mathbf{q}j_a)B_j(1,-\mathbf{q}j_a)}{\omega_{\mathbf{q}j_a}^2}. \quad (16)$$

The parameters (16) were estimated using frequencies of even and odd optical vibrations of B_g and A_u symmetry at the Brillouin zone centre of $LiLnF_4$ crystals and the corresponding coupling constants

$B_i(B_g^\upsilon)$, $B_i(A_u^\upsilon)$ which were determined earlier from the analysis of temperature and magnetic field effects in Raman scattering spectra [11] and calculated in the framework of the exchange charge model [8]. The summation over acoustic vibrations in the last term in (16) was completed by making use of the long-wave approximation that gave a possibility to connect the electron-phonon interaction constants $B_i(1,\mathbf{q}\boldsymbol{j}_a)$ with the parameters of the electron-deformation interaction (9) which were determined from piezospectroscopic measurements in [12, 13] (see table 1). The obtained values of the parameters λ_{ij} are presented in table 2.

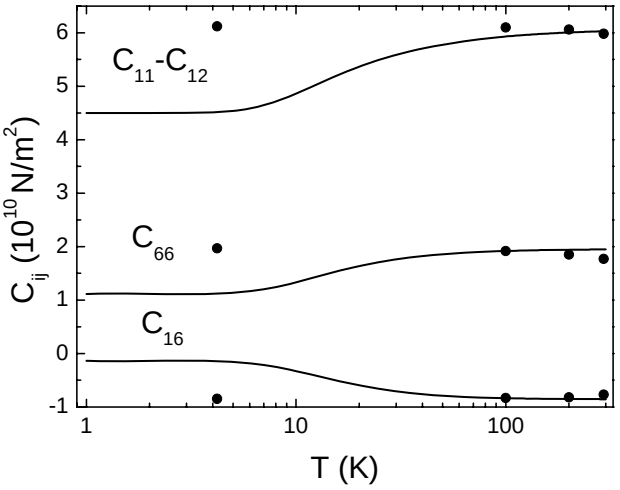

Figure 4. Calculated temperature dependences of the elastic constants in zero magnetic field. The values of the corresponding elastic constants of $LiYF_4$ are represented by symbols [15].

Relatively small corrections of the crystal field parameters obtained earlier from the analysis of the optical spectra in dilute isomorphic crystals $LiYF_4$:Dy [14] and transformed by the proper rotation of the coordinate frame around the *c*-axis [8] gave us a possibility to fit satisfactorily the measured temperature and field dependences of the magnetization in the magnetic fields parallel to the *c*-axis (see table 3). The observed not monotone behavior of the magnetization at low temperatures with the maximum close to 25 K and the minimum at 5 K (see figure 1*a*) is caused by the specific relation between the corresponding components of the *g*-tensors of the ground ($g_\parallel$=1.15) and the first excited ($g_\parallel$=5.3) crystal field sublevels of the $^6H_{15/2}$ multiplet of the Dy^{3+} ions with a gap of 24 K and the redistribution of populations of these Kramers doublets with temperature variations.

Table 3. Crystal field parameters B_p^k (cm^{-1}) for $LiDyF_4$.

p	*k*	Ref. [14]	This work
2	0	165	160
4	0	-88	-83
6	0	-4.4	-4.6
4	4	-980	-751
4	-4	0	-641
6	4	-427	-360
6	-4	-65	-243

The essential role of the electron-deformation interaction in the formation of the magnetization of the concentrated rare-earth paramagnets at low temperatures becomes apparent when analyzing the magnetization of $LiDyF_4$ induced by the magnetic fields perpendicular to the c-axis (figure 2). In this case, as it is seen in figure 2b, when accounting only for the Zeeman interaction, we obtain strongly underestimated magnetic moments of the Dy^{3+} ions in the fields exceeding 1 T.

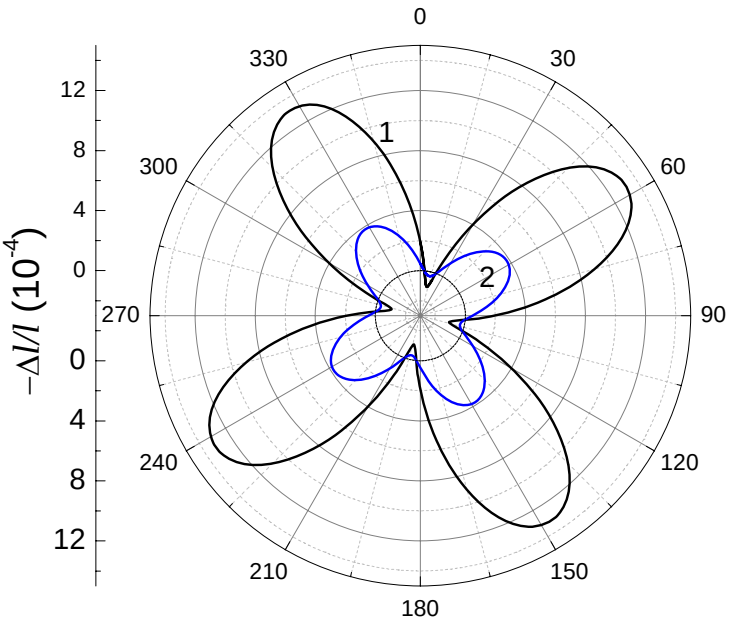

Figure 5. Calculated angular dependences of the magnetostriction in the magnetic fields B=1 T (curve 1) and 0.5 T (curve 2) , $\mathbf{B} \perp [001]$, T=4.2 K.

It should be noted that the multipole interactions bring the remarkable renormalization of the electron-deformation interaction (see table 1), and one can expect a strong softening of the $LiDyF_4$ crystal lattice similar to that observed in $DyVO_4$ [10]. The calculated temperature dependences of the elastic constants of $LiDyF_4$ which determine lattice strains induced by deformations of B_g symmetry are presented in figure 4. Indeed, the elastic constants change remarkably when the temperature decreases down to 10 K but remain almost constant at lower temperatures.

The calculated relative changes of the crystal dimensions along the magnetic field oriented in the basis plane of the crystal lattice and declined from the a-axis by the angle φ

$$\Delta l / l = e(A_g^2) + \frac{1}{2}\cos(2\varphi)e(B_g^1) + \sin(2\varphi)e(B_g^2) \qquad (16)$$

are presented in figure 5. The calculated magnetostriction is strongly anisotropic and reaches giant values of an order of 10^{-3} in the magnetic field field ~1 T at T=4.2 K. The calculated field dependence of the longitudinal magnetostriction agrees well with the experimental data (see figure 3).

4. Conclusion

The temperature and field dependences of the magnetization and field dependences of the strongly anisotropic magnetostriction in $LiDyF_4$ single crystals were measured. The giant magnetostriction of 10^{-3} was observed in rather small magnetic field of 1 Tesla directed along the [110] crystallographic axis at liquid helium temperature. The sets of parameters which define interactions of the Dy^{3+} ions with the crystal field and the crystal lattice uniform deformations as well as the parameters of the

multipole interactions between the Dy^{3+} ions were determined. The results of measurements are well reproduced by simulations. The magnetoelastic interaction in $LiDyF_4$ contributes essentially to the magnetization in external magnetic fields oriented in the basis plane of the crystal lattice at low temperatures.

Acknowledgements
The authors are grateful to V.A. Shustov for the X-Ray orientation of the samples. This work was partially supported by the RFBR grant №12-02-00372-a.

References
[1] Aminov L K, Malkin B Z and Teplov M A 1996 Magnetic properties of nonmetallic lanthanide compounds *Handbook on the Physics and Chemistry of the Rare-Earths.* **22** Amsterdam: North-Holland 295
[2] Vasyliev V, Villora E G, Nakamura M, Sugahara Y and Shimamura K 2012 *Optics Express* **20** 14460
[3] Mennenga G, de Jongh L J, Huiskamp W J and Laursen I 1984 *J. Mag. Mag. Mat.* **44** 48
[4] Kazei Z A, Snegirev V V, Chanieva R I et al. 2006 *Sol. St. Phys.* **48** 682
[5] Sokolov V I 1967 *Pribory i Tekhnika Eksperimenta (Instruments and Experimental Techniques)* **2** 181
[6] Crosswhite H M, Crosswhite H 1984 *J. Opt. Soc. Am. B* **1** 246
[7] Klekovkina V V, Zakirov A R, Malkin B Z, Kasatkina L A 2011 *J. Phys.: Conf. Ser.* **324** 012036
[8] Bumagina L A, Krotov V I, Malkin B Z, Khasanov A Kh 1981 *Sov. Phys. JETP* **54** 792
[9] Al'tshuler S A, Malkin B Z, Teplov M A, Terpilovskii D N 1985 Magnetoelastic interactions in rare-earth paramagnets $LiLnF_4$ *Soviet Scientific Reviews, Section A, Physics Reviews* **6** New York: Harwood Academic Publishers 159
[10] Elliott R J, Harley R T, Hayes W, Smith S R P 1972 *Proc. Roy. Soc. Lond. A.* **328** 217
[11] Kupchikov A K, Malkin B Z, Natadze A L, Ryskin A I 1987 *Phys. Sol. State* **29** 3335
[12] Vinokurov A V, Malkin B Z, Pominov A I, Stolov A L 1986 *Phys. Sol. State* **28** 381
[13] Bertaina S, Barbara B, Giraud R et al. 2006 *Phys. Rev. B.* **74** 184421
[14] Davidova M P, Zhdanovich S B, Kazakov B N, Korableva S L, Stolov A L 1977 *Optica i spektr.* **42** 577
[15] Blanchfield P, Saunders G A 1979 *J. Phys. C: Solid State Phys.* **12** 4673